J|A|C|S ARTICLES

Published on Web 07/21/2009

Dynamic Interplay between Spin-Crossover and Host−Guest Function in a Nanoporous Metal−Organic Framework Material

Peter D. Southon,[†] Lang Liu,[†] Elizabeth A. Fellows,[†] David J. Price,[†] Gregory J. Halder,[‡] Karena W. Chapman,[§] Boujemaa Moubaraki,[||] Keith S. Murray,[||] Jean-François Létard,[⊥] and Cameron J. Kepert*[,†]

School of Chemistry, The University of Sydney, NSW 2006, Australia, Materials Science Division and X-ray Science Division, Advanced Photon Source, Argonne National Laboratory, Argonne, Illinois 60439, School of Chemistry, Monash University, VIC 3800, Australia, and Laboratoire des Sciences Moléculaires, ICMCB (CNRS UPR 9048), Université Bordeaux I, 33608 Pessac, France

Received March 19, 2009; E-mail: c.kepert@chem.usyd.edu.au

Abstract: The nanoporous metal−organic framework $[Fe(pz)Ni(CN)_4]$, **1** (where pz is pyrazine), exhibits hysteretic spin-crossover at ambient conditions and is robust to the adsorption and desorption of a wide range of small molecular guests, both gases (N_2, O_2, CO_2) and vapors (methanol, ethanol, acetone, acetonitrile, and toluene). Through the comprehensive analysis of structure, host−guest properties, and spin-crossover behaviors, it is found that this pillared Hofmann system uniquely displays both guest-exchange-induced changes to spin-crossover and spin-crossover-induced changes to host−guest properties, with direct dynamic interplay between these two phenomena. Guest desorption and adsorption cause pronounced changes to the spin-crossover behavior according to a systematic trend in which larger guests stabilize the high-spin state and therefore depress the spin-crossover temperature of the host lattice. When stabilizing the alternate spin state of the host at any given temperature, these processes directly stimulate the spin-crossover process, providing a chemisensing function. Exploitation of the bistability of the host allows the modification of adsorption properties at a fixed temperature through control of the host spin state, with each state shown to display differing chemical affinities to guest sorption. Guest desorption then adsorption, and vice versa, can be used to switch between spin states in the bistable temperature region, adding a guest-dependent memory effect to this system.

Introduction

The achievement over the past decade of robust nanoporosity in molecular materials, most commonly in host lattices with coordination bond linkages (i.e., metal−organic frameworks; MOFs), has seen the discovery of a range of remarkable host−guest properties and led to strong interest in the application of such materials in gas storage, molecular separations and sensing, and catalysis.[1,2] A direct consequence of the considerable versatility of the molecular approach over that of more conventional porous solids is the high capacity for rational materials design, not just of framework and pore structure but of specific incorporated functions, be they sorptive, catalytic, electronic, magnetic, optical, or thermomechanical in nature. Such versatility has seen the recent targeting of systems that display some form of electronic and magnetic function,[2] which notably includes the incorporation of the spin-crossover (SCO) phenomenon[3] to yield the first switchable porous lattices.[4−8] This coupling within one material of spin switching and reversible guest exchange has provided a new, highly convenient mechanism for perturbing the structure and therefore electronic/magnetic properties of the host material, opening up a powerful new approach for the investigation of structure−property relationships in SCO systems. Moreover, differences in macroscopic properties such as magnetic moment, color, and crystal

[†] The University of Sydney.
[‡] Materials Science Division, Argonne National Laboratory.
[§] X-ray Science Division, Advanced Photon Source, Argonne National Laboratory.
[||] Monash University.
[⊥] Université Bordeaux I.

(1) Robson, R. *Dalton Trans.* **2008**, 5113–5131. Janiak, C. *Dalton Trans.* **2003**, 2781–2804. James, S. L. *Chem. Soc. Rev.* **2003**, *32*, 276–288. Eddaoudi, M.; Moler, D. B.; Li, H. L.; Chen, B. L.; Reineke, T. M.; O'Keeffe, M.; Yaghi, O. M. *Acc. Chem. Res.* **2001**, *34*, 319–330.
(2) Kepert, C. J. *Chem. Commun.* **2006**, 695–700. Kitagawa, S.; Kitaura, R.; Noro, S.-I. *Angew. Chem., Int. Ed.* **2004**, *43*, 2334–2375.
(3) Gütlich, P.; Goodwin, H. A. *Top. Curr. Chem.* **2004**, *233*, 1–47. Gaspar, A. B.; Ksenofontov, V.; Seredyuk, M.; Gütlich, P. *Coord. Chem. Rev.* **2005**, *249*, 2661–2676. Real, J. A.; Gaspar, A. B.; Muñoz, M. C. *Dalton Trans.* **2005**, 2062–2079.
(4) Halder, G. J.; Kepert, C. J.; Moubaraki, B.; Murray, K. S.; Cashion, J. D. *Science* **2002**, *298*, 1762–1765.
(5) Murray, K. S.; Kepert, C. J. *Top. Curr. Chem.* **2004**, *233*, 195–228.
(6) Neville, S. M.; Moubaraki, B.; Murray, K. S.; Kepert, C. J. *Angew. Chem., Int. Ed.* **2007**, *46*, 2059–2062. Neville, S. M.; Halder, G. J.; Chapman, K. W.; Duriska, M. B.; Southon, P. D.; Cashion, J. D.; Létard, J.-F.; Moubaraki, B.; Murray, K. S.; Kepert, C. J. *J. Am. Chem. Soc.* **2008**, *130*, 2869–2876.
(7) Halder, G. J.; Chapman, K. W.; Neville, S. M.; Moubaraki, B.; Murray, K. S.; Létard, J. F.; Kepert, C. J. *J. Am. Chem. Soc.* **2008**, *130*, 17552–17562.
(8) Quesada, M.; de la Pena-O'Shea, V. A.; Aromi, G.; Geremia, S.; Massera, C.; Roubeau, O.; Gamez, P.; Reedijk, J. *Adv. Mater.* **2007**, *19*, 1397–1402.

 10.1021/ja902187d CCC: $40.75

dimensions between the different spin states have raised questions of whether guest-induced SCO could be used as a mechanism for molecular sensing. Conversely, there has been speculation that novel host−guest properties might be achieved in these materials, either in cases where guest exchange induces SCO or where external stimuli such as temperature, pressure, magnetic field, or light irradiation could be used to switch the host lattice and allow consequent external manipulation of host−guest processes.[5]

The most extensive class of porous SCO materials yet investigated are a family of spin-crossover frameworks (SCOFs) constructed through the linkage of $Fe^{II}(py)_4(NCS)_2$ nodes by a range of bis-pyridyl ligands.[4,6,7,9] The desorption/adsorption of guest molecules into the 1-D channels of these materials has yielded a number of interesting observations, most notably the variation of SCO temperature induced by guest-exchange and the intricate complexities associated with structural transformations and their influence on SCO behavior.[6,7] To date, the tuning of ligand fields in these systems to favor SCO at ambient conditions has been elusive, meaning that the guest sorption chemistry and spin-switching principally occur in different temperature regimes and have therefore yet to be achieved simultaneously; as such, no investigations of various possible interplay between these two processes have been reported.

A further highly notable family of SCOFs is that containing $Fe^{II}(N(cyanometallate))_4(py)_2$ nodes,[10−13] some members of which display SCO at ambient temperature and pressure. Comparatively less attention has been paid to the potential host−guest aspects of these systems, with notable exceptions including the observed topochemical conversions of $[Fe^{II}(pmd)(OH_2)(M^I(CN)_2)_2]\cdot H_2O$ (pmd = pyrimidine; M = Ag, Au)[13] and $[Fe(3\text{-}CNpy)_2(CH_3OH)_{2/3}(Au(CN)_2)_2]$[14] following the thermal desorption of bound water and methanol guests, and the demonstration that desorption of unbound water from the pillared Hofmann system $[Fe^{II}(pz)Pt^{II}(CN)_4]\cdot x(H_2O)$[11] yields an increase in SCO temperature and hysteresis.[15,16] The latter material, which is a member of a series that also incorporates Ni^{II} and Pd^{II} analogues,[11,17,18] is of particular interest in displaying hysteretic SCO near room temperature and in being a likely candidate for reversible guest desorption/adsorption, given the recent report of permanent porosity in its isostructural $Ni^{II}-Ni^{II}$ analogue.[19] This SCO pillared Hofmann family has previously been the subject of considerable interest for its ambient-temperature photophysical properties[15] and for the formation of SCO nanoparticles[16,20,21] and thin films.[22] Here we show through a comprehensive guest-dependent investigation that the Ni^{II} analogue within this series, $[Fe^{II}(pz)Ni^{II}(CN)_4]\cdot x$Guest (**1**·*x*Guest; where Guest = N_2, O_2, CO_2, methanol (Me), ethanol (Et), acetone (Ac), acetonitrile (Acn), and toluene (Tol)), displays a range of remarkable and unique physicochemical materials properties, with synergistic interplay between SCO and guest-exchange leading to both guest-induced SCO and SCO-induced guest-exchange properties.

Experimental Section

Synthesis. Crystals of **1**·$2H_2O$ were obtained by the slow diffusion of stoichiometric ethanol/water (50/50) solutions of iron(II) perchlorate hydrate (21.3 mg, 0.05 mmol) and potassium tetracyanonickelate(II) and pyrazine (12.9 mg, 0.05 mmol and 4.0 mg, 0.05 mmol, respectively). Dichroic red-yellow crystals were obtained after a period of several months. Bulk samples were synthesized by fast mixing of stoichiometric amounts (8×10^{-3} M) of the three reactants in ethanol/water (50/50) and stirring for 1 day at room temperature. Fine orange-yellow powders were obtained. Elemental analysis of bulk sample ($FeNiC_8H_8N_6O_2$): found C 28.74, N 24.63, H 2.17; calcd C 28.71, N 25.11, H 2.41. IR (cm^{-1}, at room temperature): 3607s, 2145s, 1616m, 1417s, 1158m, 1130m, 1085m, 1053s, 1031m, 805s, 476m, 442s. Raman (cm^{-1}, at room temperature): 2182s, 2170s, 1605m, 1232m, 1029s, 700w, 645w, 484w, 319w, 300w, 173w. The purity of bulk samples for physical measurements was confirmed by PXRD.

Magnetic Susceptibility Measurements. Magnetic susceptibility measurements were made in the temperature range 4−300 K using a Quantum Design MPMS 5 SQUID instrument operating under a field of 1 T. All data reported were obtained on microcrystalline samples isolated, initially, as **1**·$2H_2O$. The desorbed analogue **1** was obtained by heating a sample of **1**·$2H_2O$ under a vacuum at 80 °C for 21 h. The guest-sorbed phases **1**·*x*Guest were obtained by adding a few drops of the appropriate solvent to **1** and letting the sample sit for approximately 12 h before the measurement was made. All samples were sealed under solvent in quartz tubes and were not ground at any stage. The comparatively low $\chi_M T^{LS}$ values achieved are consistent with high sample quality and purity, with only a small high-spin contribution coming from crystallite surface and defect (e.g., pz vacancy) effects. The spin-crossover temperatures $T_{1/2}^{\uparrow}$ and $T_{1/2}^{\downarrow}$ were determined as the temperatures of 50% spin-state conversion upon warming and cooling, respectively.

(9) Real, J. A.; Andres, E.; Muñoz, M. C.; Julve, M.; Granier, T.; Bousseksou, A.; Varret, F. *Science* **1995**, *268*, 265–267.

(10) Kitazawa, T.; Gomi, Y.; Takahashi, M.; Takeda, M.; Enomoto, M.; Miyazaki, A.; Enoki, T. *J. Mater. Chem.* **1996**, *6*, 119–121. Muñoz, M. C.; Gaspar, A. B.; Galet, A.; Real, J. A. *Inorg. Chem.* **2007**, *46*, 8182–8192. Agusti, G.; Muñoz, M. C.; Gaspar, A. B.; Real, J. A. *Inorg. Chem.* **2008**, *47*, 2552–2561. Martínez, V.; Gaspar, A. B.; Muñoz, M. C.; Ballesteros, R.; Ortega-Villar, N.; Ugalde-Saldívar, V. M.; Moreno-Esparza, R.; Real, J. A. *Eur. J. Inorg. Chem.* **2009**, 303–310. Galet, A.; Gaspar, A. B.; Agusti, G.; Muñoz, M. C.; Real, J. A. *Chem. Phys. Lett.* **2007**, *434*, 68–72. Galet, A.; Muñoz, M. C.; Real, J. A. *Inorg. Chem.* **2006**, *45*, 4583–4585. Galet, A.; Gaspar, A. B.; Muñoz, M. C.; Bukin, G. V.; Levchenko, G.; Real, J. A. *Adv. Mater.* **2005**, *17*, 2949–2953. Galet, A.; Muñoz, M. C.; Gaspar, A. B.; Real, J. A. *Inorg. Chem.* **2005**, *44*, 8749–8755. Niel, V.; Thompson, A. L.; Goeta, A. E.; Enachescu, C.; Hauser, A.; Galet, A.; Muñoz, M. C.; Real, J. A. *Chem.−Eur. J* **2005**, *11*, 2047–2060. Agusti, G.; Gaspar, A. B.; Muñoz, M. C.; Real, J. A. *Inorg. Chem.* **2007**, *46*, 9646–9654. Agusti, G.; Thompson, A. L.; Gaspar, A. B.; Muñoz, M. C.; Goeta, A. E.; Rodriguez-Velamazan, J. A.; Castro, M.; Burriel, R.; Real, J. A. *Dalton Trans.* **2008**, 642–649.

(11) Niel, V.; Martínez-Agudo, J. M.; Muñoz, M. C.; Gaspar, A. B.; Real, J. A. *Inorg. Chem.* **2001**, *40*, 3838–3839.

(12) Agusti, G.; Cobo, S.; Gaspar, A. B.; Molnár, G.; Moussa, N. O.; Szilagyi, P. A.; Palfi, V.; Vieu, C.; Muñoz, M. C.; Real, J. A.; Bousseksou, A. *Chem. Mater.* **2008**, *20*, 6721–6732.

(13) Niel, V.; Thompson, A. L.; Muñoz, M. C.; Galet, A.; Goeta, A. E.; Real, J. A. *Angew. Chem., Int. Ed.* **2003**, *42*, 3760–3763.

(14) Galet, A.; Muñoz, M. C.; Real, J. A. *Chem. Commun.* **2006**, 4321–4323.

(15) Bonhommeau, S.; Molnár, G.; Galet, A.; Zwick, A.; Real, J. A.; McGarvey, J. J.; Bousseksou, A. *Angew. Chem., Int. Ed.* **2005**, *44*, 4069–4073.

(16) Boldog, I.; Gaspar, A. B.; Martínez, V.; Pardo-Ibanez, P.; Ksenofontov, V.; Bhattacharjee, A.; Gütlich, P.; Real, J. A. *Angew. Chem., Int. Ed.* **2008**, *47*, 6433–6437.

(17) Molnár, G.; Niel, V.; Real, J. A.; Dubrovinsky, L.; Bousseksou, A.; McGarvey, J. J. *J. Phys. Chem. B* **2003**, *107*, 3149–3155.

(18) Molnár, G.; Niel, V.; Gaspar, A. B.; Real, J. A.; Zwick, A.; Bousseksou, A.; McGarvey, J. J. *J. Phys. Chem. B* **2002**, *106*, 9701–9707.

(19) Culp, J. T.; Smith, M. R.; Bittner, E.; Bockrath, B. *J. Am. Chem. Soc.* **2008**, *130*, 12427–12434.

(20) Volatron, F.; Catala, L.; Riviere, E.; Gloter, A.; Stephan, O.; Mallah, T. *Inorg. Chem.* **2008**, *47*, 6584–6586.

(21) Larionova, J.; Salmon, L.; Guarl, Y.; Tokarev, A.; Molvinger, K.; Molnár, G.; Bousseksou, A. *Angew. Chem., Int. Ed.* **2008**, *47*, 8236–8240.

(22) Cobo, S.; Molnár, G.; Real, J. A.; Bousseksou, A. *Angew. Chem., Int. Ed.* **2006**, *45*, 5786–5789. Molnár, G.; Cobo, S.; Real, J. A.; Carcenac, F.; Daran, E.; Vien, C.; Bousseksou, A. *Adv. Mater.* **2007**, *19*, 2163–2167.

Single-Crystal X-ray Diffraction (SCXRD). Data were collected for the crystal structures on a Bruker-Nonius FR591 Kappa APEX II diffractometer (Mo Kα radiation $\lambda = 0.71073$ Å) equipped with an Oxford Cryosystems cryostat. Data for **1** were collected on a crystal that was dehydrated *in situ* in an open-ended capillary with heating under a flow of dry dinitrogen. Empirical absorption corrections were applied using the SADABS program.[23] Solutions were obtained by direct methods using SHELXS-97 and refined with SHELXL-97.[24] Non-hydrogen atoms were refined anisotropically, and hydrogen atoms were affixed using the riding model. CCDC reference numbers: 737309−737312.

Synchrotron Powder X-ray Diffraction (S-PXRD). Diffraction patterns were collected on two beamlines at the Advanced Photon Source at Argonne National Laboratory, 11-BM ($\lambda = 0.61992$ Å) and 1-BM ($\lambda = 0.61832$ Å), using a MAR-3450 imaging plate detector. The sample temperature was controlled using an Oxford Cryosystems cryostat. Raw images were processed using Fit-2D.[25] The sample-to-detector distance and tilt of the image plate relative to the beam were refined using a LaB_6 standard. For the guest-loaded samples, polycrystalline samples of **1**·2H_2O were desorbed under vacuum at 80 °C and backfilled with dry dinitrogen, and a few drops of solvent were added. The samples were loaded into 0.5 mm glass capillaries with a small layer of solvent and flame-sealed. Data were collected in 20 s exposures with a sample−detector distance of 400 mm. For time-resolved studies, polycrystalline samples of **1**·2H_2O were ground as a slurry in a small amount of mother liquor, loaded into polyimide capillaries, immediately assembled into a flow cell apparatus,[26] and placed under a flowing helium gas atmosphere at 275 K. The samples were maintained under helium gas flow for the duration of the experiment. Diffraction patterns were collected in 5 s exposures at *ca.* 2 min intervals upon continuous ramping over the ranges 298 to 80 K, 80 to 440 K, 440 to 240 K, and 240 to 360 K, all at 180 K h^{-1}. This corresponds to the collection of diffraction images at 6 K intervals.

Lattice parameters were determined from the diffraction patterns by Rietveld refinement.[27] The starting model was based on the parameters determined from SCXRD; the tetragonal *P*4/*mmm* structural model was assumed initially, and in cases where peak-splitting due to an orthorhombic cell was clear, the *Pmmm* model was used. No attempt was made to model the disordered guest species, and consequently peak intensities were not fitted accurately in all cases.

Thermogravimetry. Measurements were carried out on a TA Instruments Hi-Res TGA 2950 thermogravimetric analyzer to determine the extent and temperature of guest desorption from **1**·2H_2O and **1**·*x*Guest (Guest = Ac, Et, Me, Tol, and Acn); samples of the latter were generated by the *ex situ* immersion of **1** in the relevant pure solvent. The temperature was ramped to 170 °C at 1 °C min^{-1} to desolvate the materials, which were loaded wet to prevent guest desorption prior to measurement.

Gas and Vapor Adsorption. Adsorption isotherms and isobars for **1** were measured using an IGA-002 gravimetric adsorption instrument (Hiden-Isochema, UK). For all isotherms the sample temperature was maintained within ±0.1 °C. The standard error for each weight reading was typically 0.25 μg, leading to error bars considerably smaller than the data points shown below in Figures 5a,b, 6, and 8; e.g., for the CO_2 isotherms the median error was 0.014% of the absorbed mass. Reproducibility and sample integrity were confirmed by the collection of repeat isotherms and isobars, both on different samples and on samples that had been cycled with multiple guests.

CO_2 (99.99%) isotherms were measured to 2.5 bar at a range of temperatures between 283 and 318 K, and N_2 (99.99%) isotherms were measured to 10 bar at a range of temperatures between 278 and 327 K. At each temperature (except the maximum and minimum temperatures), isotherms were measured once after cooling from the maximum temperature and once after warming from the minimum temperature to explore the influence of thermal history on spin state and adsorption properties. Enthalpy of adsorption calculations were carried out using the virial method[28] with the Clausius−Clapeyron relation on data collected as single series of isotherms and are described fully in the Supporting Information.

Gas adsorption isobars were measured for N_2 (0.5, 1, 2, 5, and 10 bar), O_2 (0.5, 1, 2, 5, and 10 bar), and CO_2 (0.1, 0.2, 0.5, 1, and 2 bar) by maintaining the pressure of the gas in the chamber while increasing the temperature at 0.1 K min^{-1} from 275 to 313 K and then cooling back to 275 K. The order of pressure measurements was randomized to confirm that sample history did not influence the pressure-dependent properties.

Vapor adsorption isotherms for ethanol, toluene, acetone, and methanol were measured at 30 °C at pressures up to 0.9 of the saturation pressure (P_0). At each measured pressure, the sample weight was monitored until the equilibrium mass was achieved. The adsorption isotherm for acetonitrile was not measured due to incompatibility with instrument materials.

Adsorption isotherms for N_2 (77 K) and Ar (87 K) on **1** were measured using a Micromeritics ASAP2020 volumetric instrument.

Raman Spectroscopy. Data were recorded on a Renishaw Raman InVia Reflex spectrometer equipped with a 2.2 mW argon ion 514.5 nm laser (Modu-Laser, Centerville, UT) and a Linkam THMS 600 temperature stage. Spectra were collected at *ca.* 20 K above and below the $T_{1/2}^{\uparrow}$ and $T_{1/2}^{\downarrow}$ respectively, with sample sealed in 0.5 mm glass capillary tubes under a thin layer of solvent.

Optical Reflectivity. Data were collected using a custom-built setup that allows reflectivity spectra to be collected from 450 to 950 nm in the temperature range 10−300 K. The measurements were performed directly on a thin layer of a polycrystalline sample with a small amount of guest solvent added to avoid desorption.

Results

Structure and Properties of 1·2H_2O. The structure adopts the general topology reported previously,[11] consisting of 2-D $FeNi(CN)_4$ layers bridged through the six-coordinate Fe(II) centers by bis-unidentate pyrazine bridges (Figure 1). From a non-twinned crystal the material was determined to crystallize in the orthorhombic space group *Pmmm*, rather than in the tetragonal space group *P*4/*m* as determined previously from an *ab initio* structure derived from PXRD data.[11] The majority of crystals measured were found to be merohedrally twinned, yielding *a* and *b* parameters that represent averaged values within an apparent tetragonal lattice; datasets collected on these crystals yielded excellent structural refinements in *P*4/*mmm* with 50:50 occupation of orthogonal pz orientations but were refined instead in *Pmmm* with a twin relation (Table 1). The Fe−N bond lengths for two structures obtained at 150 K (non-twinned and twinned) and one at 300 K of $Fe-N_{cyanide} = 1.944(3)$ Å,

(23) Sheldrick, G. M. *SADABS. Empirical adsorption correction program for area detector data*; University of Göttingen, Germany, 1996.
(24) Sheldrick, G. M. *SHELXL-97. Program for crystal structure refinement*; University of Göttingen, Germany, 1997.
(25) Hammersley, A. P. ESRF Internal Report, 1997. Hammersley, A. P.; Svensson, S. O.; Hanfland, M.; Fitch, A. N.; Hausermann, D. *High-Pressure Res.* **1996**, *14*, 235–248.
(26) Chupas, P. J.; Chapman, K. W.; Kurtz, C.; Hanson, J. C.; Lee, P. L.; Grey, C. P. *J. Appl. Crystallogr.* **2008**, *41*, 822–824. Chupas, P. J.; Ciraolo, M. F.; Hanson, J. C.; Grey, C. P. *J. Am. Chem. Soc.* **2001**, *123*, 1694–1702.
(27) Larson, A. C.; von Dreele, R. B. *General Structure Analysis System (GSAS)*; Los Alamos National Laboratory Report LAUR 86-748; Los Alamos National Laboratory: Los Alamos, NM, 2000. Toby, B. H. *J. Appl. Crystallogr.* **2001**, *34*, 210–213.
(28) Chen, B.; Zhao, X.; Putkham, A.; Hong, K.; Lobkovsky, E. B.; Hurtado, E. J.; Fletcher, A. J.; Thomas, K. M. *J. Am. Chem. Soc.* **2008**, *130*, 6411–6423.

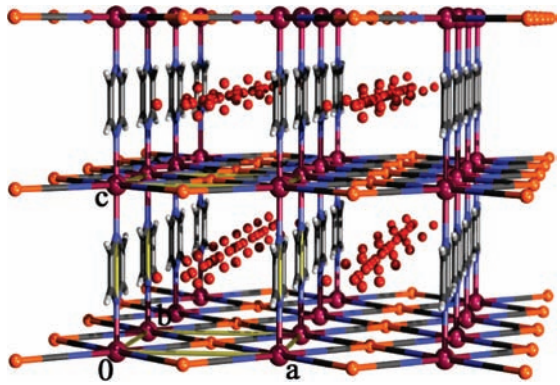

Figure 1. Orthorhombic crystal structure of $\mathbf{1}\cdot 2H_2O$. 1-D channels propagate along the *b* axis between the pyrazine pillared $FeNi(CN)_4$ grids and are filled with disordered water molecules.

$Fe-N_{pyrazine} = 1.986(3)$ Å (150 K non-twinned), $Fe-N_{cyanide} = 1.946(5)$ Å, $Fe-N_{pyrazine} = 1.971(5)$ Å (150 K twinned), and $Fe-N_{cyanide} = 2.128(4)$ Å, $Fe-N_{pyrazine} = 2.226(6)$ Å (300 K) are indicative of low-spin (LS) and high-spin (HS) Fe^{II} centers, respectively (Table 2).[29]

Careful analysis of the residual electron density in the 1-D channels of the untwinned structure uncovered four principal atom sites, making identification of the guests highly ambiguous. Reasonable refinements of both this and the twinned datasets were obtained by constraining the channel composition to be two disordered H_2O molecules per formula unit (Figure 1), consistent with our microanalysis and thermogravimetric results and generally consistent with previous reports of this compound.[11,17,21]

The SCO behavior of $\mathbf{1}\cdot 2H_2O$ is shown in Figure 2. Corresponding S-PXRD data show the progress of the discontinuous transformation between the HS and LS phases, with there being no intermediate phases observed (Figure 3a,b). The temperature dependence of the lattice parameters refined from both S-PXRD and SCXRD data matches the SCO behavior seen in the magnetic data (see Supporting Information).

Guest Desorption. With complete guest desorption to yield the apohost **1**, there is a symmetry change to a tetragonal cell with $a' = b' \approx a$ and $c' \approx c$. SCXRD analysis of this phase (Table 1) reveals that the tetragonal symmetry describes a dynamic rotation of the pyrazine bridges. S-PXRD data collected during desorption of a rapidly synthesized powder sample of $\mathbf{1}\cdot 2H_2O$, from which splitting of *a* and *b* was unable to be resolved, confirms little change in the refined lattice parameters with guest desorption (see Table 3, below).

Careful analysis of the S-PXRD data collected during guest desorption from $\mathbf{1}\cdot 2H_2O$ to **1** indicates the emergence and disappearance of at least two superstructure phases. The first of these involves the emergence of diffuse diffraction peaks at *ca.* 7.7 and 14.2° (see Supporting Information), consistent with a structural transformation to a tetragonal supercell with $\mathbf{a}'' = \mathbf{a} - \mathbf{b}$, $\mathbf{b}'' = \mathbf{a} + \mathbf{b}$, and $\mathbf{c}'' = \mathbf{c}$, i.e., giving $a'' = b'' \approx \sqrt{2}\,a$ and $c'' \approx c$. The systematic absences are consistent with a transformation to the space group *P*4/*mbm*, which suggests that there is a 90° rotation of alternating pyrazine bridges within the structure (Figure 4b). Such an arrangement seems likely to correspond to a 50% desorbed phase $\mathbf{1}\cdot 1H_2O$, in which the two pore water molecules occupying 1D channels in $\mathbf{1}\cdot 2H_2O$ convert to a situation were one pore water molecule occupies larger pores at the higher temperature. In contrast to the fully solvated orthorhombic phase, in which the pyrazine bridges lie parallel throughout the untwinned structure, as affected by distortion of the rhombic grid layers, no such interlayer correlation is expected for this tetragonal case. This is consistent with the relatively diffuse nature of the superstructure reflections, which are expected to exist as rods rather than points in reciprocal space due to the 2-D intralayer order.

The SCO transition in **1** is considerably sharper and has wider hysteresis than that of $\mathbf{1}\cdot 2H_2O$, as evidenced both by magnetometry (Figure 2) and S-PXRD (Figure 3c,d). No intermediate phases were observed, and the temperature-dependent lattice parameters refined from the S-PXRD data closely match the SCO behavior observed magnetically (see Supporting Information).

Adsorption of Gases. When gas adsorption isotherms are measured at temperatures in the bistable temperature range (i.e., within the SCO hysteresis loop), the spin state of the host has a substantial effect on the gas isotherms. Figure 5a,b shows CO_2 and N_2 isotherms measured at 298 K, after either cooling from above 320 K to obtain the HS state or warming from below 280 K to obtain LS. Further isotherms for a range of temperatures between 278 and 327 K are given in the Supporting Information. From these isotherms, values for the enthalpy of adsorption (ΔH_{ads}) were calculated (see Figure 5c,d). For CO_2 adsorption, $\Delta H_{ads} = 30$ kJ/mol at low loading for both the HS and LS states, and for the LS state it increases slightly with increasing loading to be *ca.* 2 kJ/mol greater than that for HS. In contrast, N_2 is adsorbed more favorably into the HS state, with ΔH_{ads} at low loadings of 16 kJ/mol for HS and 14 kJ/mol for LS. In most cases ΔH_{ads} was seen to increase with guest sorption, suggesting that a small degree of framework distortion occurs to optimize the host−guest interactions.

The adsorption isobars of N_2, O_2, and CO_2 display remarkable hysteretic behaviors that arise directly from the structural changes associated with SCO (Figure 6); to our knowledge, such behaviors have not been seen previously for porous materials. Superimposed on a general trend of decreased gas adsorption at higher temperatures are hysteretic features arising from abrupt spin switching of the host lattice. For N_2 and O_2 the adsorption capacity for $\mathbf{1}^{HS}$ is greater than that for $\mathbf{1}^{LS}$. For CO_2 adsorption the effect of spin state on adsorption capacity is pressure dependent; at higher pressures the behavior is similar to N_2 and O_2, but at lower pressures (<0.5 bar) $\mathbf{1}^{LS}$ has a slightly higher adsorption capacity.

The hysteresis loops observed closely match the magnetic SCO behavior, but with some subtle shifts in temperature. The isotherm SCO temperatures $T_m^{\uparrow}$ and $T_m^{\downarrow}$ were defined for each isobar as the temperature corresponding to the maximum rate of mass change during heating and cooling, respectively; these are expected to correlate very closely with, but not necessarily equate exactly to, $T_{1/2}$ values determined by magnetic measurement. Values of T_m are plotted against amount adsorbed in Figure 7. For N_2 and O_2 adsorption, there is a nearly linear relationship between the hysteretic SCO temperatures and the extent of loading. For $\mathbf{1}\cdot x N_2$, linear fitting of the T_m data gives the relationships $T_m^{\uparrow}/K = 294.7 - 13.9x$ and $T_m^{\downarrow}/K = 304.7 - 12.3x$; for $\mathbf{1}\cdot x O_2$, $T_m^{\uparrow}/K = 294.3 - 4.9x$ and $T_m^{\downarrow}/K = 304.3 - 2.7x$. In contrast, the dependence of T_m values on CO_2 loading shows no simple linear trend.

The adsorption isotherms for N_2 and Ar gas on **1** were also measured at 77 and 87 K, respectively. The type I isotherms

(29) Guionneau, P.; Marchivie, M.; Bravic, G.; Létard, J.-F.; Chasseau, D. *Top. Curr. Chem.* **2004**, *234*, 97–128.

Table 1. Crystal Data and Refinement Details for **1**·2H_2O and **1**

		1·2H_2O		**1**
formula		$C_8H_8N_6O_2FeNi$		$C_8H_4N_6FeNi$
FW/g mol^{-1}		334.76		298.73
T/K	150	150[a]	300[a]	375
spin state	LS	LS	HS	HS
crystal system	orthorhombic	orthorhombic	orthorhombic	tetragonal
space group	*Pmmm*	*Pmmm*	*Pmmm*	*P*4/*mmm*
a/Å	7.1139(3)	7.016(1)	7.2666(3)	7.2574(13)
b/Å	6.9109(4)	7.019(1)	7.2696(3)	7.2574(13)
c/Å	6.7799(3)	6.785(1)	7.2421(3)	7.256(3)
V/Å^3	333.32(3)	334.16(9)	382.57(3)	382.17(17)
ρ_{calc}/Mg m^{-3}	1.668	1.664	1.453	1.298
μ/mm^{-1}	2.502	2.496	2.180	2.164
data/restraints/parameters	585/1/38	561/1/36	688/1/37	365/0/22
$R_1(F^2)$ [$I > 2\sigma(I)$, all]	0.0334, 0.0394	0.0362, 0.0688	0.0393, 0.0541	0.0464, 0.0993
$wR_2(F^2)$ [$I > 2\sigma(I)$, all]	0.0885, 0.0936	0.0779, 0.0943	0.1083, 0.1200	0.0969, 0.1182
GoF	1.118	1.153	1.227	0.962

[a] Merohedrally twinned structures; the a and b parameters determined from these collections are partially averaged due to this twinning.

Table 2. Selected Bond Lengths and Other Structural Parameters for **1**·2H_2O and **1**

		1·2H_2O		**1**
T/K	150	150[a]	300[a]	375
$\langle d_{Fe-N(C)}\rangle$/Å	1.944(3)	1.946(5)	2.128(4)	2.117(6)
$\langle d_{Fe-N(pz)}\rangle$/Å	1.986(3)	1.971(5)	2.226(6)	2.213(12)
pore diameter/Å	3.72	3.62	3.87	3.86
pore volume/%	29.9	29.9	35.2	35.1

[a] Merohedrally twinned structures.

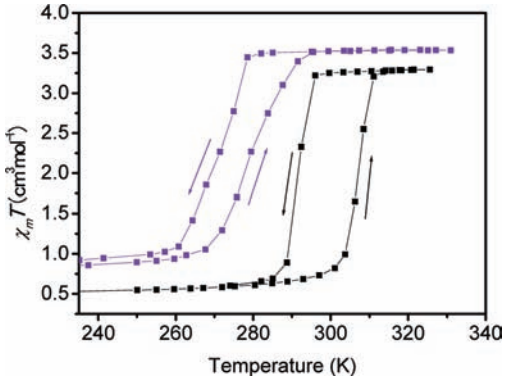

Figure 2. Temperature dependence of $\chi_M T$ for **1**·2H_2O (violet) and **1** (black).

observed with abrupt adsorption at very low pressure are typical for ultramicroporous materials (see Supporting Information for further details).

Vapor/Liquid Adsorption. The methanol, ethanol, and acetone vapor adsorption isotherms showed fully reversible, abrupt uptake at very low pressure (Figure 8). Maximum uptake into the pores, as measured at $0.8P_0$ (above this value it is probable that there will be condensation of surface solvent), corresponded to approximately 1.8, 1.5, and 1.2 guest molecules per formula unit for methanol, ethanol, and acetone, respectively. The stoichiometry decreases with increasing molecular size, as expected. These stoichiometries are in fair agreement with those determined by thermogravimetric desorption of **1** exposed to liquid solvent, which gave values of *ca.* 1.6, 1.5, 1.1, 1.0, and 0.8 for ethanol, methanol, acetone, acetonitrile, and toluene, respectively. Values listed in Table 3 are taken from vapor adsorption except for the value for acetonitrile, which is incompatible with the adsorption equipment. With the exception of toluene vapor (see Supporting Information), each of these guests undergoes very fast adsorption kinetics, with time constants less than 60 s. Toluene adsorption increased steadily to 0.6 toluene molecule per unit cell at $0.8P_0$, with two regions of slow kinetics suggestive of framework rearrangement most likely associated with rotation of the pz pillars.

Variable-temperature magnetic susceptibility measurements were used to probe the spin states and spin changes of **1**·*x*Guest (Figure 9), revealing pronounced guest dependence in the SCO properties, both transition temperatures and hysteresis widths. Table 3 contains the $T_{1/2}^{\downarrow}$ (cooling) and $T_{1/2}^{\uparrow}$ (warming) values and corresponding hysteresis widths.

The Rietveld-refined lattice parameters for the guest-loaded phases are given in Table 3. Interestingly, peak splitting of the $\langle hhl\rangle$ reflections was clearly observed for **1**·1.5Et^{LS} and **1**·1.0Acn^{LS}, indicating the host lattice returns to the parent orthorhombic symmetry rather than retaining the tetragonal symmetry of the apohost. All other patterns were indexed accurately to 2θ angles in tetragonal *P*4/*mmm*, suggesting that the pz pillars are aligned perpendicularly or randomly within these phases; we note also that merohedral twinning of an orthorhombic structure may lead to formally tetragonal crystallites, and that the data may be of insufficient resolution to distinguish very closely similar a and b.

Optical Reflectivity. The absorption spectra of **1**·*x*Guest show a reversible conversion between HS (absorption minimum at *ca.* 670 nm) and LS states (minimum at *ca.* 800 nm) upon cooling and warming (see Figure 10 for **1**·1.2Ac). SCO temperatures derived from these variable-temperature data are in very close agreement with those obtained from the magnetic data (see Supporting Information for data on all phases).

Discussion

Structure and Properties of 1·2H_2O. The synthesis of single crystals of **1**·2H_2O—a notoriously difficult task for pillared Hofmann systems of this type—has allowed the first unambiguous structural characterization of this phase, revealing an orthorhombic structure in which the Hofmann-type $FeNi(CN)_4$ layers are slightly distorted away from a regular square grid (rhombic angle = 2arctan(b/a) = 88.3° at 150 K) and the interlayer pyrazine pillars align parallel throughout the structure.

(30) Webster, C. E.; Drago, R. S.; Zerner, M. C. *J. Am. Chem. Soc.* **1998**, *120*, 5509–5516.
(31) Personal communication with M. L. T. Jordan; see Supporting Information for details.

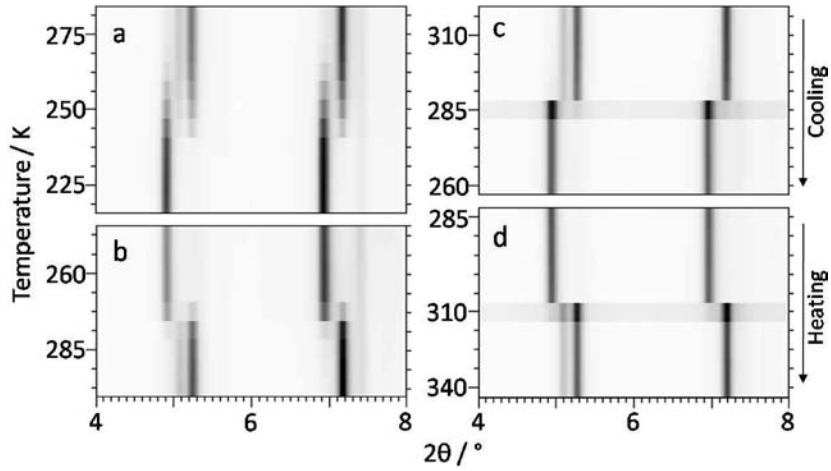

Figure 3. Evolution of S-PXRD reflections versus temperature for **1**·2H_2O (a,b) and **1** (c,d) upon cooling and warming through the hysteretic SCO transition: peaks at *ca.* 5° are the overlap of [100], [010], and [001]; peaks at *ca.* 7° are the overlap of [110], [101], and [011]. The regions of SCO are clearly discernible as discontinuities.

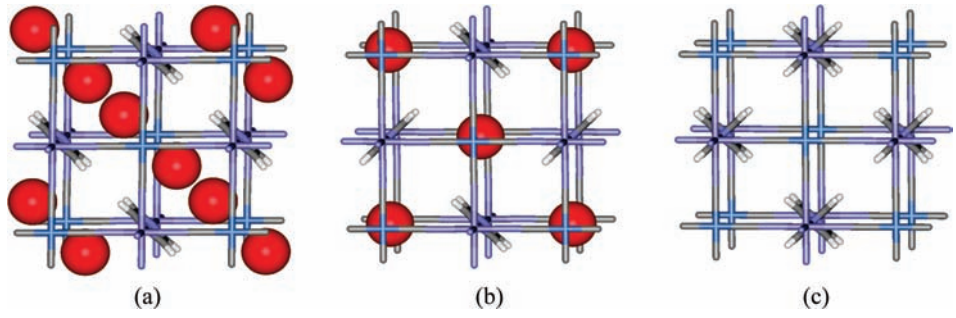

Figure 4. Structural transformations associated with desorption from **1**·2H_2O (a; orthorhombic *Pmmm*) to **1**·1H_2O (b; proposed tetragonal *P*4/*mbm*) to the apohost **1** (c; tetragonal *P*4/*mmm*). Red spheres represent water molecules.

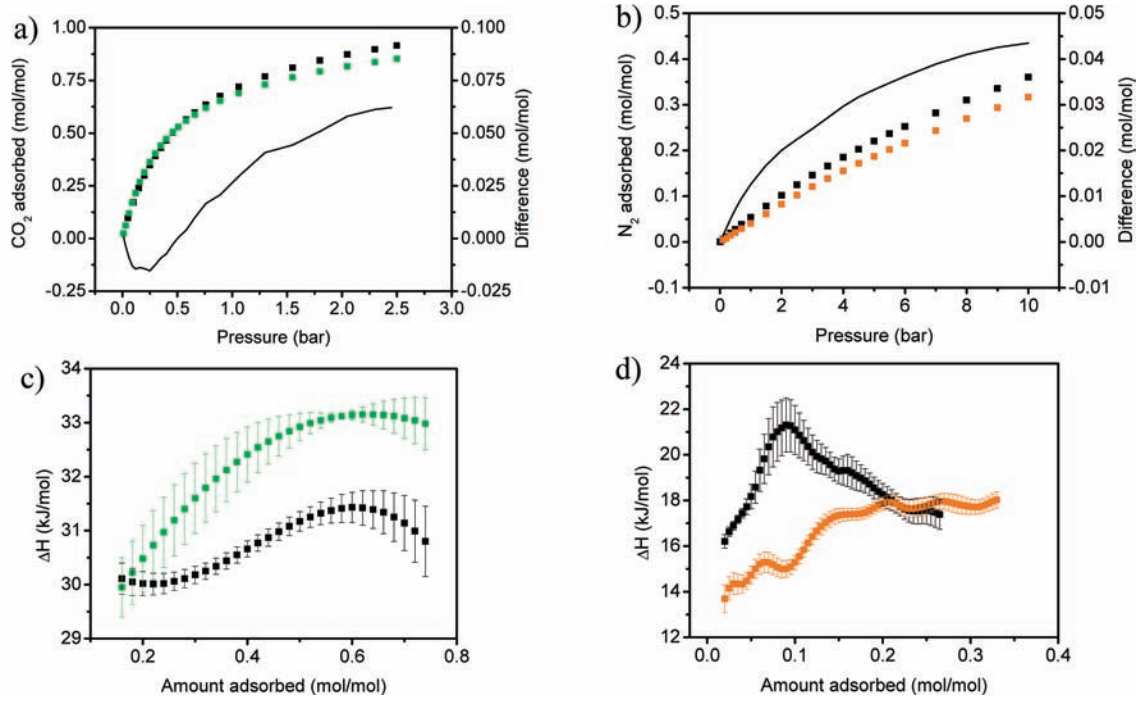

Figure 5. (a) CO_2 and (b) N_2 adsorption isotherms for $\mathbf{1}^{HS}$ (black squares) and $\mathbf{1}^{LS}$ (green and orange squares, respectively) at 298 K. The solid line shows the difference between the isotherms for $\mathbf{1}^{HS}$ and $\mathbf{1}^{LS}$. Enthalpy of adsorption for CO_2 (c) and N_2 (d) onto $\mathbf{1}^{HS}$ (black) and $\mathbf{1}^{LS}$ (green and orange squares, respectively). Error bars (±1 esd) are determined from fits to the adsorption isosteres.

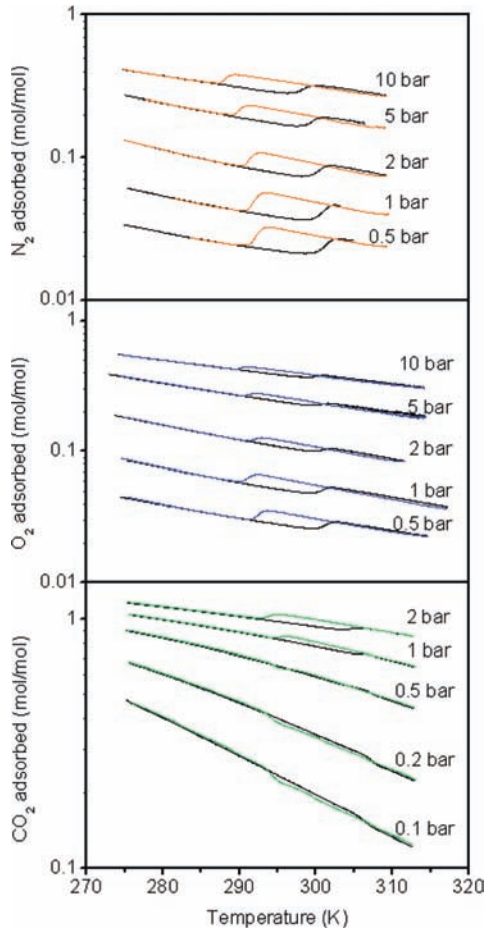

Figure 6. N_2, O_2, and CO_2 adsorption and desorption isobars for **1** collected upon warming (black data points) and cooling (orange, blue, and green, respectively).

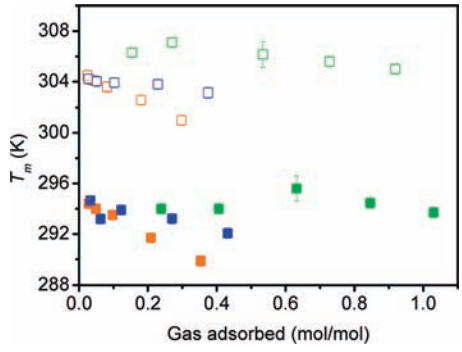

Figure 7. Dependence of the hysteretic SCO temperatures $T_m^{\uparrow}$ (open symbols) and $T_m^{\downarrow}$ (filled symbols) on the extent of loading of the gases N_2 (orange), O_2 (blue), and CO_2 (green). The LS → HS transitions are shown as filled symbols, and the HS → LS transitions as open symbols. Error bars are shown at ±1 esd.

This structural ordering contrasts with the random alignment of the pyrazine bridges reported previously within tetragonal structures of this phase[11] and is likely driven by weak pyrazine−cyanide repulsion and/or framework−guest interactions to favor the long-range grid distortion. Due to the lack of communication of pyrazine orientation between interlayers, and to the nearly orthogonal geometry of the rhombic $FeNi(CN)_4$ grids, the structure is highly susceptible to merohedral twinning along the *c* direction. For rapidly synthesized powder samples, this twinning appears to occur at the nanoscale, as confirmed

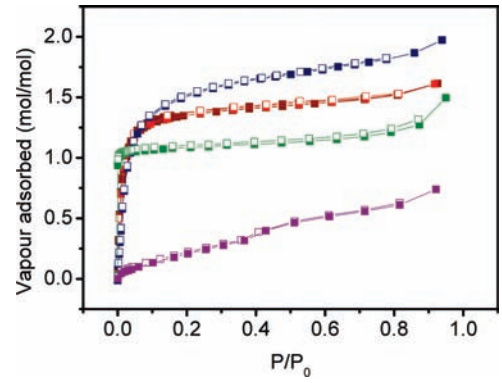

Figure 8. Vapor adsorption isotherms for **1**: methanol (blue), ethanol (red), acetone (green), and toluene (purple). The molar adsorption is given with respect to the host formula $[Fe(pz)Ni(CN)_4]$.

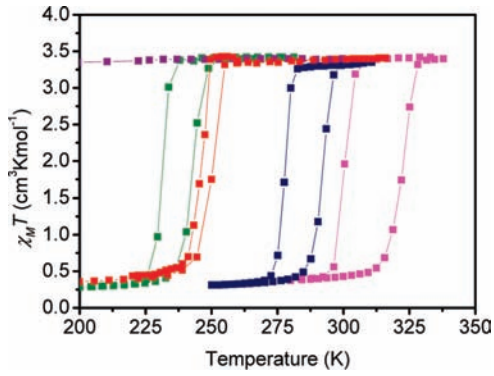

Figure 9. Temperature dependence of $\chi_M T$ for **1**·0.6Tol (purple), **1**·1.2Ac (green), **1**·1.5Et (red), **1**·1.8Me (blue), and **1**·1.0Acn (pink).

by the absence of any observable distinction of the *a* and *b* axes in S-PXRD patterns and the refinement of *ca.* 50:50 twin components in the orthorhombic refinement of merohedrally twinned crystals. As such, an interesting feature of this material is that twinned crystallites have a different framework geometry from untwinned, with the rhombic grid layers constrained by crystal strain to be locally orthogonal.

Sample inhomogeneity associated with the crystal twinning likely explains the relatively broad SCO transition observed. Notably, we obtained magnetic behavior for this phase similar but not identical to that reported previously,[11] with the differences likely due to a different degree of solvation and/or extent of twinning. The discontinuous nature of the SCO transition in **1**·$2H_2O$, with the absence of any apparent loss of S-PXRD peak intensity at the transition, indicates that no crystalline intermediates exist and that SCO occurs essentially instantaneously within each crystallite; a previous micro-Raman mapping investigation of this material has suggested that the distribution of HS and LS domains at the transition is submicrometer in scale.[32] This situation is in contrast to that seen in the SCOF phases,[4,6,7] where gradual shifts in the diffraction reflections are observed as the Fe(II) sites cross over continuously rather than simultaneously within each crystallite.[4,6,7] We attribute this comparatively rare case of a truly abrupt transition to the fact that partial SCO would induce considerable strain unless occurring in a regular fashion throughout the crystallite (e.g., as a checkerboard arrangement of HS and LS sites; notably, such an effect has

(32) Molnár, G.; Bousseksou, A.; Zwick, A.; McGarvey, J. J. *Chem. Phys. Lett.* **2003**, *367*, 593–598.

Table 3. SCO Temperatures, Hysteresis Widths (ΔT), Guest Dimensions and Volumes,[30,31] and Refined Lattice Parameters from S-PXRD for **1**·*x*Guest, where Guest = Water, None, Acetone (Ac), Ethanol (Et), Methanol (Me), Acetonitrile (Acn), and Toluene (Tol)

	1·2H_2O	**1**	**1**·1.2Ac	**1**·1.5Et	**1**·1.8Me	**1**·1.0Acn	**1**·0.6Tol
$T_{1/2}^{\uparrow}$	278	307	243	251	292	322	HS
$T_{1/2}^{\downarrow}$	270	287	236	246	278	300	HS
ΔT	8	20	8	5	14	22	n/a
guest vol./Å^3	19.7	0	64.4	60.0	40.9	52.3	101.3
guest dim./Å^3	3.2	0	6.6	6.2	5.2	4.7	6.6
	×2.9		×4.1	×4.8	×4.5	×4.0	×4.0
	×3.9		×5.2	×4.3	×4.7	×4.0	×8.2
a/Å (HS)	7.2693(5)	7.2562(10)	7.2623(12)	7.2574(4)	7.2551(8)	7.2694(10)	
c/Å (HS)	7.2441(7)	7.2371(14)	7.2109(15)	7.2471(5)	7.2379(11)	7.2288(12)	
V/Å^3 (HS)	382.80(5)	381.06(9)	380.32(13)	381.70(4)	380.98(8)	382.00(10)	
T/K (HS)	277	348	270	340	340	350	
a/Å (LS)	7.0282(6)	7.0131(6)		7.0726(11)	7.0194(7)	7.0966(15)	
b/Å (LS)				6.9700(12)		6.930(2)	
c/Å (LS)	6.7970(8)	6.7762(7)		6.7925(5)	6.7848(8)	6.7683(8)	
V/Å^3 (LS)	335.74(7)	333.28(6)		334.84(5)	334.30(7)	332.92(7)	
T/K (LS)	202	242		200	200	240	

recently been seen to occur via continuous SCO transitions in two-step SCO transitions in 1-D chain[33] and 2-D grid[7] SCO systems). As such, any broadening of the transition as observed by other bulk techniques arises from sample inhomogeneity rather than, for example, guest molecule disorder and its local influence on the Fe(II) environment. The most likely causes of this bulk inhomogeneity are crystallite twinning and variation in guest composition, a point that is supported by the considerable sharpening of the transition following guest desorption; such an effect demonstrates also that the SCO broadening is not caused by crystal size distribution effects.

Guest Desorption. Desorption of water guests from **1**·2H_2O to yield the apohost **1** results in a transformation to a tetragonal structure in which the pyrazine units are now dynamically disordered over two orthogonal orientations (perpendicular to *a* or *b*) and the rhombic $FeNi(CN)_4$ grids formally adopt a square geometry. Powder diffraction data collected upon cooling of **1** show no evidence for a conversion back to the orthorhombic symmetry. These data provide no information on whether short- or long-range ordering of the pz units, either parallel or perpendicular, might occur upon cooling, but given their large separation it seems most likely that these units will freeze into random orientations to retain the formally tetragonal symmetry.

In situ S-PXRD measurement with heating shows that the desorption transformation occurs via at least one intermediate. This most notably includes the formation of a proposed ($\sqrt{2}$, $\sqrt{2}$,1) supercell with partial desorption from **1**·2H_2O to **1**·1H_2O, involving the rotation of alternating pyrazine bridges. This results in a change to the pore structure, with the 1-D channels in the *b*-direction being converted into a 2-D pore architecture in the *ab*-plane with slightly enlarged pores in the vicinity of the Ni atoms (Figure 11); the width of the windows between the pyrazine units decreases from 4.2 to 2.6 Å in the *ab*-plane, while the total calculated pore volume[34] of 35% is unchanged by the transformation. This proposed intermediate appears to be stabilized principally by the optimization of host−guest $H_2O\cdots\pi$(pz) interactions with increasing kinetic volume of the guest water molecule, rather than by the formation of edge-to-face pz···pz interactions (calculated C−H···π(pz) distance = 5.34 Å for perpendicular pz alignment); the latter are expected to be extremely weak, consistent with the absence of this structural modulation in **1** down to 80 K. Notably, the rotation of the pz pillars results in the blockage of the very narrow (1.9 × 1.9 Å^2) windows that pass through the alternating holes in the square grid layers; windows of this size have been shown to allow migration of small guests such as H_2O.[35]

The modification of the SCO properties upon desorption of **1**·2H_2O is very similar to that reported for the Pt analogue, $[Fe(pz)Pt(CN)_4]\cdot xH_2O$ ($x = 0, 2$),[15] with a *ca.* 20−30 K increase in transition temperature, a *ca.* 10 K broadening of the hysteresis loop, and a pronounced sharpening of the transition; these data suggest that some SCO properties previously assigned to **1**·2H_2O[11,32] had inadvertently been measured following a degree of water desorption. We attribute the increase in transition temperature to two factors: an increased ligand field strength arising from the conversion to a more regular Fe(II) geometry within the now square $FeNi(CN)_4$ grids of **1**, and the stabilization of the LS state through removal of what seem to be unfavorably

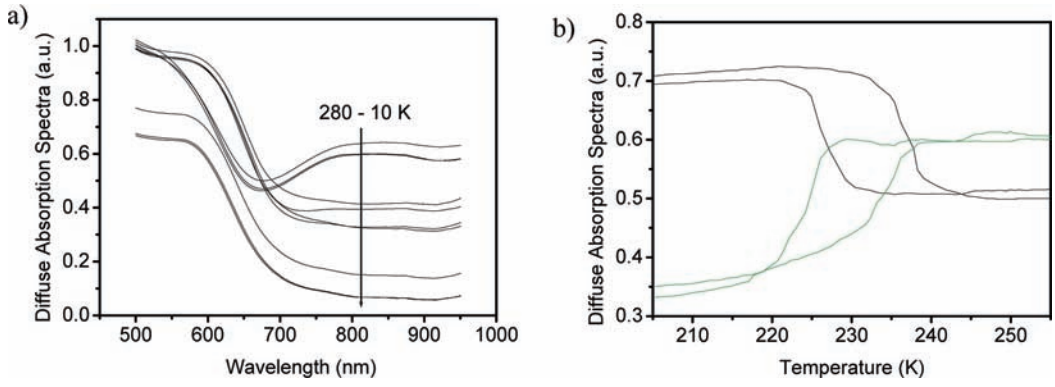

Figure 10. (a) Diffuse absorbance spectra of **1**·1.2Ac collected in the temperature range 10−280 K upon cooling and (b) absorbance at 830 nm (green) and 647 nm (black).

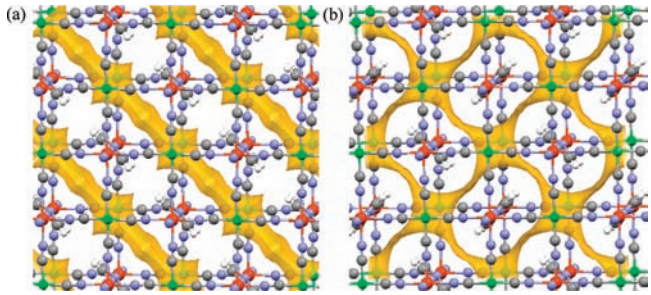

Figure 11. Modification of the framework (ball-and-stick) and pore (orange surface) structure with transformation from $\mathbf{1}\cdot 2H_2O$ (a) to $\mathbf{1}\cdot 1H_2O$ (b; proposed structure).

short $OH_2\cdots\pi$(pz) interactions for the LS state (as evidenced by the widening of the 1-D channels in the untwinned structure of $\mathbf{1}\cdot 2H_2O^{LS}$, which has $a > b$; see Table 1 and Figure 1). The sharpening of the SCO transition is likely due principally to the removal of crystallite twinning with conversion to tetragonal symmetry, and possibly also to the removal of sample inhomogeneity associated with varying guest solvation between different crystallites. Notably, the hysteresis loop of this phase is now centered at ambient conditions, providing a rare example of a SCO material that displays bistability at room temperature.

Adsorption of Gases. The robust porous apohost phase **1** readily adsorbs a wide range of small molecular guests. At low temperatures, N_2 and Ar saturation are reached at low pressures to yield $\mathbf{1}\cdot 2N_2$ and $\mathbf{1}\cdot 2$Ar. Isotherm measurements within the bistable temperature region show that the adsorption properties of **1** depend on its spin state, with $\mathbf{1}^{LS}$ taking up less N_2 gas at 298 K than its HS counterpart (Figure 5b). We attribute this novel effect principally to the substantial decrease in pore size and volume from $\mathbf{1}^{HS}$ to $\mathbf{1}^{LS}$, which arises due to the *ca.* 0.2 Å contraction in Fe−N bond distances (Table 2). To our knowledge, this is the first example of a material where the adsorption properties at a fixed temperature can be modified by exploiting framework bistability, in this case of electronic origin. Remarkably, this effect is seen also in the adsorption isobars of N_2 and O_2 (Figure 6), in which the SCO hysteresis is mirrored in the temperature-dependent adsorption behavior. A notable feature of these data is that crossover from $\mathbf{1}^{HS}$ to $\mathbf{1}^{LS}$ leads to the expulsion of guests upon cooling, indicating that the energetics of SCO are sufficient in magnitude to drive this process.

While the SCO energetics are sufficient to influence guest sorption/desorption, it is clear that the converse is also true, with gas adsorption seen to cause subtle changes to the SCO behavior. This is consistent with the comparable energetics of each process, with the adsorption enthalpies of *ca.* 15−20 kJ mol^{-1} for N_2 and *ca.* 30 kJ mol^{-1} for CO_2 (see Figure 5c,d) being similar in scale to the SCO energies reported for $\mathbf{1}\cdot 2H_2O$ (ΔH_{SCO} = 14.5 kJ mol^{-1}, ΔS_{SCO} = 51 J K^{-1} mol^{-1}).[18] Close examination of the gas isobar data shows that adsorption of the weakly interacting N_2 and O_2 guests causes a slight suppression of the SCO transition temperature (Figure 7). This behavior is opposite in sign to and greater in magnitude than that expected for the application of external pressure[17,36,37] and is perhaps most readily interpreted as being due to an internal pressure effect in which host−guest repulsion slightly disfavors conversion from $\mathbf{1}^{HS}$ to $\mathbf{1}^{LS}$, the latter of which has smaller pores. This conclusion is consistent with the higher enthalpy of N_2 physisorption for $\mathbf{1}^{HS}$ over that of $\mathbf{1}^{LS}$. Fitting of the isobar data shows that, for N_2 adsorption, the SCO temperatures $T_m^{\uparrow}$ and $T_m^{\downarrow}$ are each suppressed by *ca.* −13 K per molar N_2 uptake, whereas for O_2 there is only a *ca.* −3 K suppression per molar uptake. This trend matches that of the guest width, with O_2 having slightly smaller van der Waals radii (2.985 × 2.930 × 4.052 $Å^3$) than N_2 (3.054 × 2.991 × 4.046 $Å^3$).[30] The influence of the smaller size of the O_2 molecule is also seen in its greater relative uptake into both $\mathbf{1}^{HS}$ and $\mathbf{1}^{LS}$ at comparable pressures and temperatures. We note that interaction of the paramagnetic (presumed triplet state) O_2 guests with the HS Fe(II) centers may also serve in some way to influence energetics of gas adsorption and SCO, although this is expected to be a minor effect at most.

Intriguingly, the adsorption of CO_2 yields significantly more complex behavior than does that of N_2 and O_2, indicating a more complex influence of guest sorption on framework structure. First, we note that CO_2 adsorption is favored into $\mathbf{1}^{LS}$ at low loadings (<0.5 mol/mol) and into $\mathbf{1}^{HS}$ at high loadings, as is seen both in the crossing-over of the $\mathbf{1}^{LS}$ and $\mathbf{1}^{HS}$ isotherms (Figure 5a) and in the inversion of the hysteretic isobars (Figure 6). This behavior appears to be caused by two competing influences: a *ca.* 2 kJ mol^{-1} higher enthalpy of adsorption for CO_2 into $\mathbf{1}^{LS}$ than into $\mathbf{1}^{HS}$ (Figure 5c), and a higher saturation loading of CO_2 into $\mathbf{1}^{HS}$. The latter is due presumably to the greater porosity of the HS phase, and possibly also to its greater framework flexibility, which may be important should some degree of structural rearrangement be required to optimize packing at higher loadings. We speculate that the enthalpically preferred adsorption of CO_2 (dimensions 3.339 × 3.189 × 5.361 $Å^3$)[30] into $\mathbf{1}^{LS}$ arises with the "sandwiching" of this longer guest between parallel pz units, for which the separation appears more optimal in $\mathbf{1}^{LS}$ (pz$\cdots$pz separation = 7.01 Å) than in $\mathbf{1}^{HS}$ (7.27 Å).

In addition to this unusual uptake-dependent behavior, a nonlinear influence of CO_2 adsorption on SCO temperature is observed. Unlike N_2 and O_2, the adsorption of CO_2 causes an initial slight increase in $T_m^{\uparrow}$ and $T_m^{\downarrow}$, likely reflecting a stabilization of the LS state by an internal compressive effect associated with the proposed (pz)$\pi\cdots CO_2\cdots\pi$(pz) interactions; this is consistent with the higher adsorption enthalpy seen for $\mathbf{1}^{LS}$. At higher CO_2 loadings the downward trend in SCO temperatures, as seen also for N_2 and O_2, occurs despite the higher adsorption enthalpy into $\mathbf{1}^{LS}$ at these loadings and possibly reflects an internal pressure effect as CO_2 docks into other regions of the pores.

A highly noteworthy aspect of the gas sorption isobars is that the sharpness of the SCO transitions is retained for partial gas loadings, with the deviation in SCO temperature between different loadings being greater than the broadening seen at any given loading. This feature arises naturally from the fact the SCO transition occurs abruptly within single crystallites and, hence, is influenced by bulk crystallite composition rather than solely by local second coordination sphere effects, with the latter being expected to cause SCO broadening in partially adsorbed crystallites were this not the case.

(33) Neville, S. M.; Leita, B. A.; Halder, G. J.; Kepert, C. J.; Moubaraki, B.; Létard, J. F.; Murray, K. S. *Chem.—Eur. J.* **2008**, *14*, 10123–10133.
(34) Spek, A. L. *Acta Crystallogr.* **1990**, *A46*, 194–201.
(35) Goodwin, A. L.; Chapman, K. W.; Kepert, C. J. *J. Am. Chem. Soc.* **2005**, *127*, 17980–17981.
(36) Gütlich, P.; Ksenofontov, V.; Gaspar, A. B. *Coord. Chem. Rev.* **2005**, *249*, 1811–1829.
(37) Meissner, E.; Koppen, H.; Spiering, H.; Gütlich, P. *Chem. Phys. Lett.* **1983**, *95*, 163–166.

Adsorption of Vapors/Liquids. At ambient temperatures, methanol, ethanol, acetone, acetonitrile, and toluene vapors are readily adsorbed into the host lattice. Guest adsorption causes subtle changes to the framework structure, as evidenced by S-PXRD measurement, with there being evidence in some cases for conversion back to the orthorhombic phase (Table 3); this likely indicates that the pz pillars are able to realign to regenerate the 1-D pore structure of Figure 11a.

The adsorption of vapors/solvents into **1** causes significantly more pronounced changes to the SCO properties than gases, yielding a remarkable series of behaviors in which the SCO varies within a 100 K range or is "turned off" completely. We attribute this enhanced guest dependence over that of gaseous guests to the greater energetics of adsorption associated with stronger host−guest interactions, which are able to more strongly perturb the energetics of the SCO lattice. Notably, the guest dependence observed is more extreme than that seen to date in the SCOF series,[4,6,7] for which comparable guest exchange leads to a *ca.* 60 K variation in SCO temperature in cases where there is no significant lattice distortion. The more pronounced temperature dependence seen for **1**·*x*Guest likely arises due to the smaller pores of this host material, for which SCO leads to greater relative changes in pore dimensions and pore volume. Perhaps more importantly, the 2-D grids of this phase are likely to be highly intolerant to the varying spatial needs of the adsorbed guests on account of their relative inflexibility; in contrast, the dipyridyl bridging ligands in SCOF phases have been shown to lengthen upon crossover from HS to LS to partially compensate for the decrease in pore dimensions caused by Fe−N bond length contraction.[7] Such pronounced guest dependence, coupled with potential guest selectivity, makes frameworks of this Hofmann type interesting candidates for molecular sensing applications.

For the six solvent guests investigated, we see an approximately monotonic relationship between guest dimensions and SCO temperature, with the larger guests leading to a greater suppression of the switching transition (Table 3). This relationship provides one of the first tangible methods to engineer SCO systems with prescribed properties, a point that is discussed in detail below. As with the weakly interacting gas sorptives, this can be conveniently rationalized as being due to an internal pressure effect in which larger guests stabilize $\mathbf{1}^{HS}$ over $\mathbf{1}^{LS}$ due to their binding being less optimal in the smaller pores of $\mathbf{1}^{LS}$; as noted previously, evidence for the optimization of host−guest interaction energies is seen in the widening (and shortening) of the 1-D channels in the untwinned 150 K structure of $\mathbf{1}\cdot 2H_2O^{LS}$ (Figure 1 and Table 1). One interesting exception to this size-dependent trend is the increase of the SCO temperature seen with the sorption of Acn into **1**. We speculate that Acn, the narrowest of the large solvent guests (see Table 3), like CO_2, may dock most favorably between parallel pz units of the LS structure, thereby stabilizing $\mathbf{1}\cdot 1.0Acn^{LS}$ over $\mathbf{1}\cdot 1.0Acn^{HS}$ due to an internal compressive effect arising from (pz)$\pi\cdots$Acn$\cdots\pi$(pz) interactions that are absent in **1**.

It is interesting to note that no clear trend exists between SCO temperatures and framework vibrational frequencies (see Supporting Information), with the latter providing some measure of the changes to the Fe(II) ligand field with differing guests. This suggests that variation in the ligand field splitting at the SCO centers has a comparatively minor influence on the overall lattice energetics, with the dominant temperature-dependent energy term being crystal packing effects associated with optimization of host-guest interactions. As such, we believe that variation of the second-sphere Fe(II) interactions plays a relatively minor role, and that it is the bulk steric considerations of guest docking that principally determine the SCO temperature. This effect can be rationalized as arising with the decrease in effective kinetic dimensions of the guests with decreasing temperature (an internal pressure effect arising with the decreased thermal population of anharmonic longitudinal host−guest vibrations), reaching a point at some temperature where pore contraction associated with crossover at the Fe(II) centers becomes favorable due to more optimal guest binding. Interestingly, such a guest-size-dependent effect has yet to be seen in the larger-pore SCOF systems,[4,6,7] for which less pronounced guest dependence is seen. Notably, the delineation of such a simple size-dependent structure−property relationship for a SCO system, which allows the SCO properties to be engineered in a predictable fashion, has eluded attempts over many years. This situation is in stark contrast, for example, to the crystal chemisty of discrete SCO systems, for which crystal packing energetics are considerably more tolerant to SCO; for such materials, a principal influence on SCO properties of the guest species is the modification of the ligand field strength through very subtle and largely unpredictable changes in crystal packing interactions, making the deconvolution and subsequent control of these effects very difficult.[38]

While we observe a systematic trend in SCO temperature with guest size, no clear relationship exists with SCO hysteresis width, which varies considerably for the different guests. This point alone is of considerable interest in demonstrating that intraframework 'communication" effects, whether they be steric or electronic in nature, do not solely govern the bistable temperature range. With the extent of electronic and structural bistability in SCO systems depending on factors such as the rate of change in energy of the HS and LS states with temperature and the activated solid-state pathway between these, this suggests that the energetics of the HS and LS crystalline states vary differently with temperature for the different guests (i.e., that the SCO enthalpies show some temperature dependence and/or that the SCO entropies show some guest-dependence) and/or, perhaps more likely, that the guest molecule influences the energetics of the activated pathway taken between each crystalline state. The latter mechanism in particular is expected to be influenced by factors such as the effective rate of change of kinetic dimensions of the guests with temperature. We note also that the lack of any trend in the hysteresis width with SCO temperature indicates that the thermal energy of the sample does not appear to strongly influence the temperature range of bistability.

Memory Effects. The adsorption of all guests investigated in this study was found to be entirely reversible, with guest desorption yielding the apohost structure **1** in all cases. Such a property is conventional for robust framework materials of this type. Exploitation of the framework's bistability, however, allows this reversibility to be formally broken in an extremely novel fashion: at 297 K, sorption then desorption of Acn in $\mathbf{1}^{HS}$ occurs via the process $\mathbf{1}^{HS} \rightarrow \mathbf{1}\cdot 1.0Acn^{LS} \rightarrow \mathbf{1}^{LS}$, whereas adsorption then desorption of Ac in $\mathbf{1}^{LS}$ occurs via the process $\mathbf{1}^{LS} \rightarrow \mathbf{1}\cdot 1.2Ac^{HS} \rightarrow \mathbf{1}^{HS}$ (see Supporting Information). In each case, the framework does not return reversibly to its initial form, instead retaining memory of the spin state of the solvated phase. Similarly, guest-sorbed phases are able to retain a memory of

(38) Hostettler, M.; Tornroos, K. W.; Chernyshov, D.; Vangdal, B.; Bürgi, H. B. *Angew. Chem., Int. Ed.* **2004**, *43*, 4589–4594.

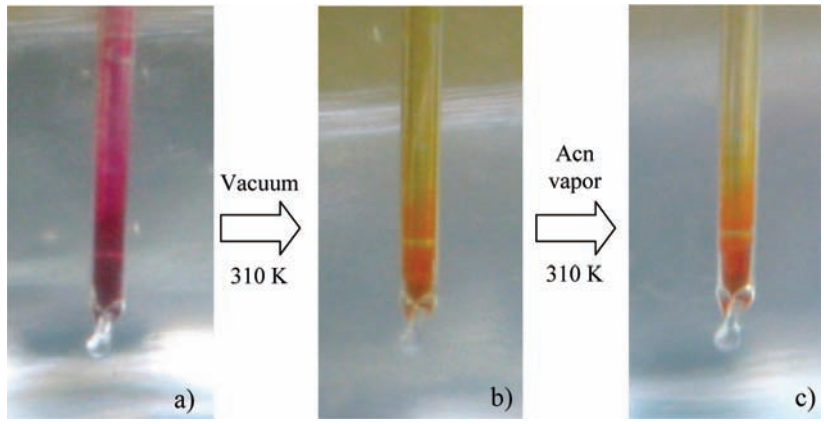

Figure 12. Isothermal desorption then resorption of Acn at 310 K: (a) $\mathbf{1}\cdot x\text{Acn}^{LS} \rightarrow$ (b) $\mathbf{1}^{HS} \rightarrow$ (c) $\mathbf{1}\cdot x\text{Acn}^{HS}$. The first step shows a guest-desorption-induced SCO from LS (purple) to HS (yellow).

their desorbed state: desorption then resorption of $\mathbf{1}\cdot 1.0\text{Acn}^{LS}$ at 310 K proceeds via the process $\mathbf{1}\cdot 1.0\text{Acn}^{LS} \rightarrow \mathbf{1}^{HS} \rightarrow \mathbf{1}\cdot 1.0\text{Acn}^{HS}$ (Figure 12). This novel property is made possible by the fact that the energetics of guest sorption/desorption and migration are insufficient to excite the host lattice between its HS and LS states within the bistable temperature region. As such, this material not only is able to act as an "instantaneous" molecular sensor but within the bistable temperature region can remember its spin state prior to guest adsorption/desorption. This adds a further unique sensing functionality to materials of this type.

Conclusions

We report highly novel guest-dependent SCO properties and spin-state-dependent host−guest properties in a robust pillared Hofmann-type system. The adsorption of molecular guests in this system occurs with sufficient energy to significantly perturb the energetics of SCO, thereby yielding dramatic changes to the SCO properties; this effect is particularly pronounced for the more strongly interacting solvent guests. Due to this, and to the fact that guest adsorption/desorption and SCO switching uniquely occur in the same temperature and pressure regimes, we are able to demonstrate conclusively that guest adsorption/desorption can induce SCO, thereby joining the well-established quartet of temperature,[39] pressure,[37] magnetic field,[40] and light irradiation[41] as SCO stimuli. Such a property, which is highly specific for each of the guests studied, points to possible molecular sensing applications for systems of this type and to the possible generation of more advanced materials functionalities in which guest exchange is used to stimulate materials function (e.g., electronic, magnetic, optical, chemical, mechanical, etc.) in a switchable fashion.

Changes to the SCO behavior of this system may be rationalized uniquely in terms of a simple guest size/shape argument; in addition to external pressure[37] and particle size effects,[16,20,21,42] this relationship provides one of the first clear routes toward the engineering of prescribed SCO switching properties, some 78 years after the first report of this switching phenomenon.[39] Our systematic analyses suggest that this simple relationship, which in essence is an extension of the external pressure effect that has been widely documented for the SCO phenomenon,[12,37,43] exists because the dominant factor that determines the temperature of SCO is the temperature-dependent host−guest interaction energies rather than guest-induced variations to ligand field splittings at the SCO centers or other similarly subtle effects. Clearly, the "internal pressure" rationalization put forward represents a considerable oversimplification, with the adsorbed guests applying anisotropic interactions spread non-uniformly across the pore surfaces rather than bulk isotropic pressure/compression internally. As such, further guest-exchange measurements and structural analyses, coupled with guest binding simulations, will be of great interest to better delineate this effect and to elucidate more sophisticated structure−property relationships that incorporate details of the guest shape and its orientation within the pores rather than simply its relative dimensions. The exploration of partial guest loading and mixtures of guests, which is expected to lead to intermediate SCO temperatures if the SCO energetics are determined principally by the optimization of temperature-dependent host−guest interactions, is likely to be particularly illuminating.

The observation of alternate preferential adsorption of different guests into this porous host lattice in its different spin states, shown here as a relatively minor effect for N_2 and CO_2, suggests that new molecular separation strategies may be possible for switchable hosts. For example, such materials could potentially be used to alternately adsorb/desorb two different guests from a mixture through control of the host spin state. Moreover, such systems might provide useful for the separation of three-component mixtures through exploitation of the differential guest selectivities of the HS and LS states of the host.

While the adsorption of molecular guests in this system occurs with sufficient energy to perturb the energetics of SCO, it is most interesting that the energetics of guest adsorption/desorption and guest migration processes do not, under the adsorption/desorption conditions explored here, provide sufficient impetus to excite the crystallites to their alternate spin state if performed within the bistable temperature region. This feature, coupled with the fact that this is the first material reported for which guest adsorption/desorption and SCO switching occur in the

(39) Cambi, L.; Szego, L. *Ber. Dtsch. Chem. Ges.* **1931**, *B64*, 259.
(40) Qi, Y.; Muller, E. W.; Spiering, H.; Gütlich, P. *Chem. Phys. Lett.* **1983**, *101*, 503–505.
(41) Decurtins, S.; Gütlich, P.; Köhler, C. P.; Spiering, H.; Hauser, A. *Chem. Phys. Lett.* **1984**, *105*, 1.
(42) Forestier, T.; Mornet, S.; Daro, N.; Nishihara, T.; Mouri, S.; Tanaka, K.; Fouche, O.; Freysz, E.; Létard, J. F. *Chem. Commun.* **2008**, 4327–4329.
(43) Simaan, A. J.; Boillot, M. L.; Carrasco, R.; Cano, J.; Girerd, J. J.; Mattioli, T. A.; Ensling, J.; Spiering, H.; Gütlich, P. *Chem.−Eur. J* **2005**, *11*, 1779–1793.

same temperature range, means that the host lattice is able, in certain temperature ranges, to retain memory of its spin state through guest sorption/desorption processes. Most notably, we show that exploitation of the host lattice bistability leads to highly novel spin-state-dependent sorption isotherms and hysteretic sorption isobars and to sample history-dependent molecular sensing properties. To our knowledge, this represents the first exploitation of host bistability to control adsorption properties.

To conclude, synergistic interplay between SCO and guest-exchange processes means that both guest-exchange-induced SCO and SCO-induced guest-exchange properties are exhibited by this system. In addition to further mapping out these highly novel effects, it will be interesting to explore whether interplay with other SCO stimuli might produce other, even more exotic materials properties. For example, laser irradiation at temperatures within the SCO hysteresis region is known to excite this framework phase between the HS and LS spin states,[15] raising the very interesting question of whether such an effect could be used to stimulate the uptake or release of guests within a light-induced adsorbent and/or release agent.

Acknowledgment. This work was supported by an ARC Discovery Project Grant (DP0557000), the French-Australia Science & Technology (FAST) Program (FR050129), the Australian Institute of Nuclear Science and Engineering (Postgraduate Research Award to E.A.F.), and the Australian Synchrotron Research Program, which is funded by the Commonwealth of Australia under the Major National Research Facilities Program. Work done at Argonne National Laboratory and use of the Advanced Photon Source was supported by the U.S. Department of Energy, Office of Science, Basic Energy Sciences, under Contract No. DE-AC02-06CH11357. We thank Peter L. Lee and Nadia Leyarovska for beamline support, Simon S. Iremonger for assistance with gas sorption measurements, Cédric Desplanches for assistance with optical reflectivity measurements, and Meredith L. T. Jordan for the calculation of guest dimensions.

Supporting Information Available: Additional magnetic susceptibility, optical reflectivity, vibrational spectroscopic, thermogravimetric, S-PXRD, and gas and vapor adsorption data, crystallographic information files and special refinement details, ORTEP diagrams, optical photography, and guest dimension calculations. This material is available free of charge via the Internet at http://pubs.acs.org.

JA902187D